CHAPTER 4

Model Verification and Simplified Model of the 10 kW_{th} Solar-Absorption Heat Transformer Combining with a Vapor Compression Heat Pump

4.1 Introduction

This chapter is to set up an experiment to verify the developed model of a 10 kW_{th} solar H_2O-LiBr absorption heat transformer (AHT) integrating with a vapor compression heat pump (VCHP) presented in the previous chapter. The VCHP is used to recover rejected heat at the AHT condenser and transfers back to the AHT evaporator. The AHT unit takes low temperature heat from a solar hot water heater having a set of flat-plate solar collectors in parallel connection each having an area of 2.3 m^2 with $F_R(\tau\alpha)$ and F_RU_L of 0.802 and 10.37 $W/m^2 \cdot K$, respectively. With this approach, input heat form solar collectors could be supplied at the AHT generator only. For the VCHP, in this part, a single-stage R-123 refrigerants and a cascade type of R-134a and R-123 refrigerants are considered. Moreover, a simplified model of the solar-AHT and the solar-CAHT are developed. The system simulations are calculated with the weather data of Chiang Mai, Thailand.

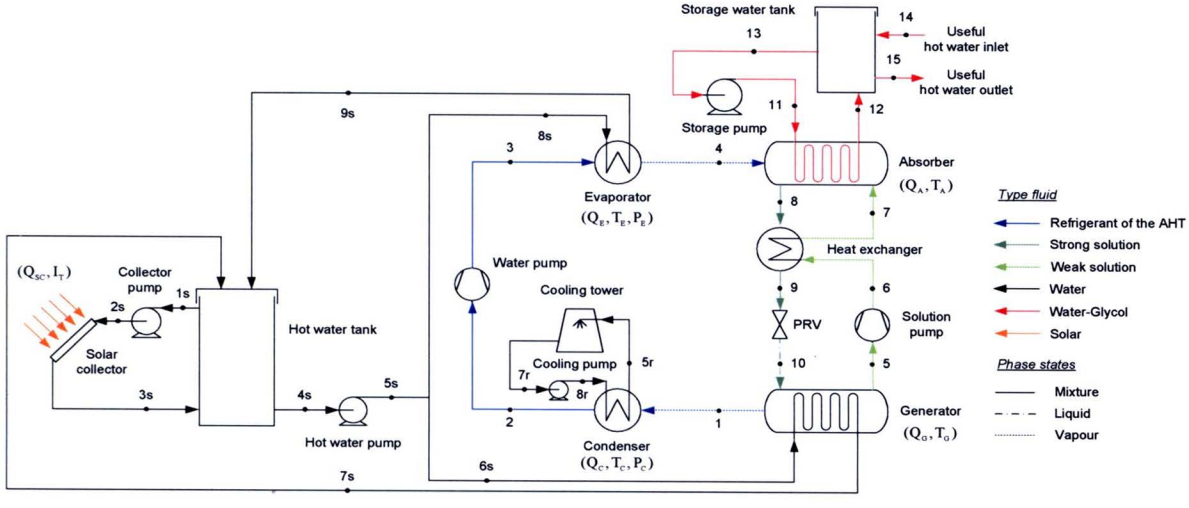

Figure 4.1 Schematic diagram of a solar absorption heat transformer.

4.2 System Descriptions and Thermodynamic Performance

Figure 4.1 shows a schematic sketch of a solar-absorption heat transformer (solar-AHT). Solar heat is supplied to the AHT generator and evaporator at a medium temperature (around 60-80 °C) and rejected heat at a lower temperature (around 35-45 °C) at the AHT condenser. A higher temperature heat (around 90-120 °C) is obtained at the AHT absorber. The basic equations of each component in the AHT cycle as presented in the previous study could be used to simulate the temperature profile and the overall COP of the AHT cycle as shown in Figure 3.12. The solar radiations (I_T) and the weather data of Chiang Mai, Thailand (RETScreen Data, 2010 and Thai Meteorological Department, 2010) are taken as the input data. It could be found that the maximum temperature in the cycle was absorber temperature (T_A) and the overall COP was not over 0.5.

When a VCHP is combined to the AHT cycle (CAHT) to recover the heat rejected from the AHT condenser which is supplied back to the AHT evaporator, the solar heat could be supplied at the AHT generator only. For the simulation in the previous chapter, it could be found that the overall COP was increased from 0.5 to 0.8.

4.3 Verification of the Simulation Results with the Experimental Data

For the experimental procedures, the constructed AHT is tested its thermal performances to upgrade heat from the installed flat-plate solar collectors. The details of the positions of the measuring sensors and the testing procedures are shown as Appendix E. The objective of this experiment is to verify data with the simulation results and to find out the thermal performances of the absorption system which the performance data of the solar-AHT and solar-CAHT are shown as Appendix F.

For the experiments, a set of 10 unit solar collectors each in parallel connection and an auxiliary heater of 10 kW were integrated with a 1,500 liter of hot water tank for supplying heat to the absorption system. It could be seen that the boosted temperature of the CAHT in term of gross temperature lift (GTL) between the absorber temperature (T_A) and the evaporating temperature (T_E) could be increased around 25.61 °C compared with 15.98 °C of the AHT. The condenser temperature (T_C)

of the CAHT was lower than the AHT around 6.15 °C. When T_C of the CAHT was low then the pressure and the temperature of the generator decreased thus the solar heat could be supplied at the generator more effectively. All the results were shown in Figure 4.2. It could be seen that the generator temperature of the CAHT was lower than that of the AHT. Figure 4.3 also shows the H_20-LiBr concentration in the AHT cycles and the overall COPs. It could be seen that the simulated results agreed quite well with the experimental data.

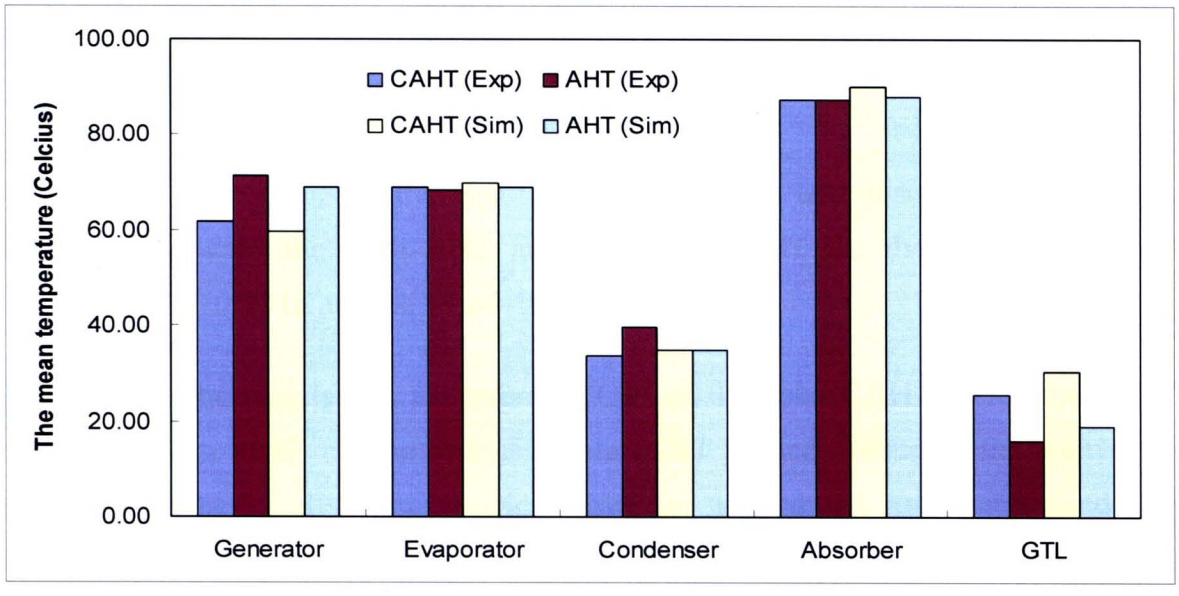

Figure 4.2 Comparisons of the working fluid temperature of each component between the solar-AHT and the solar-CAHT for the testing results on 15/10/2010 at time 13:30-15:30.

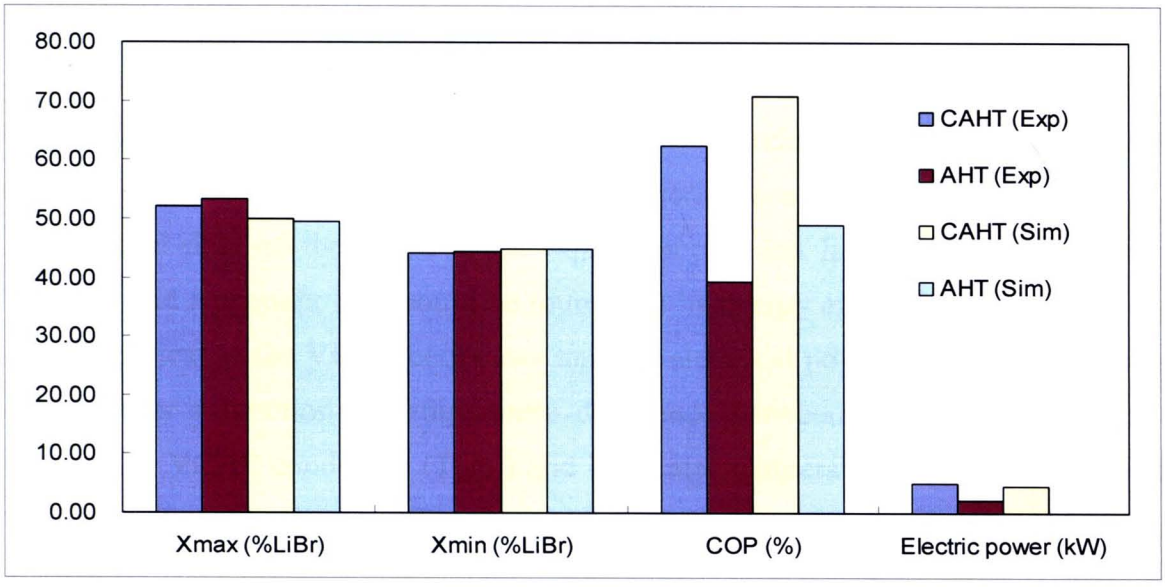

Figure 4.3 Comparisons of the H_20-LiBr concentration and absorption performance between the solar-AHT and the solar-CAHT for the testing results on 15/10/2010 at time 13:30-15:30.

From the simulation, the overall COPs of the solar-CAHT were around 0.71 compared with 0.49 of the normal Solar-AHT which included the conversion efficiency at the VCHP from electrical power to mechanical power at around 60%. For the experimental results, the overall COPs of solar-CAHT and the solar-AHT were around 0.62 and 0.39, respectively.

4.4 Simplified Models

In this study, a single-stage vapor compression heat pump having R-123 as refrigerant has been used to recover heat at the AHT condenser which is upgraded and transferred to the AHT evaporator. The specifications of each component and the experimental data of the single-stage vapor compression heat pump are shown in Table 4.1 and Appendix E. It could be found that its energy efficiency ratio (EER_{VCHP} - a ratio of heat at the VCHP condenser and the electrical power consumption) could be set up as a function of temperature difference between the water temperature entering the VCHP condenser ($T_{HW,i}$) and the water temperature entering the VCHP evaporator ($T_{CW,i}$) as shown in Figure 4.4, the empirical correlations could be found in forms of

$$EER_{VCHP} = -0.0816(T_{HW,i} - T_{CW,i}) + 4.6483, (kW_{th}/kW_e), \quad (4.1)$$

Similarly, for the supplied power for the compression work

$$W_{VCHP} = 0.0041(T_{HW,i} - T_{CW,i}) + 1.7198, (kW_e). \quad (4.2)$$

Table 4.1 Descriptions of each component of the single-stage VCHP.

Devices	Properties
Compressor (Scroll compressor)	Power input 1.50 A Displacement volume 12.7 m^3/h
Evaporator (Plate heat exchanger)	Capacity 8.00 kW Area 1.64 m^2
Condenser (Plate heat exchanger)	Capacity 10.00 kW Area 1.64 m^2
Expansion valve (Thermo static orifice 02)	Capacity 10.00 kW Pressure ratio 3.00

In the study, to get higher performance, a two-stage VCHP, having R-134A and R-123 refrigerants for low pressure and high pressure has also been taken. The specifications of each component of the two-stage vapor compression heat pump are shown in Table 4.2.

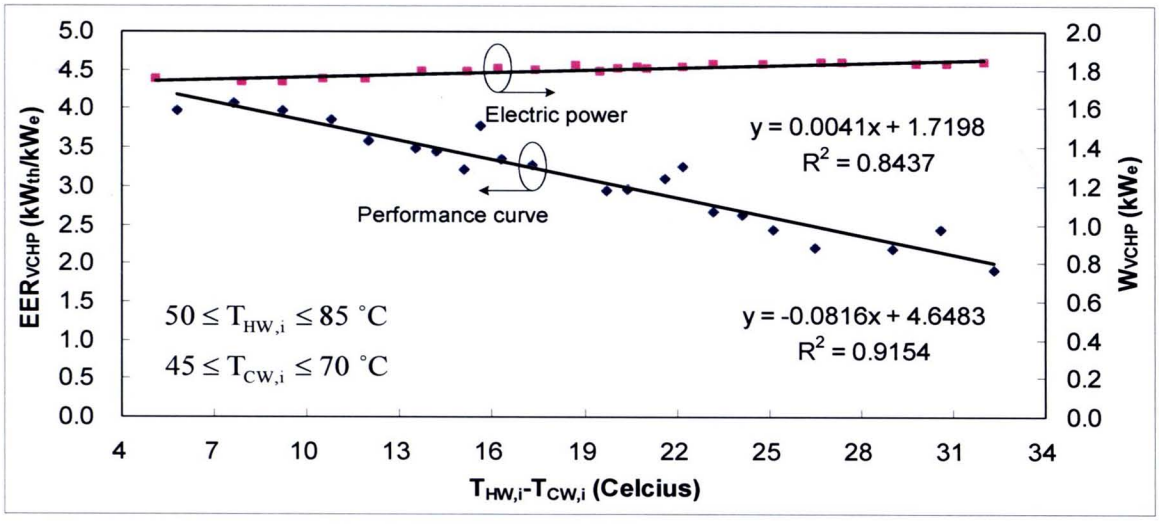

Figure 4.4 Performance curves of the R-123 single-stage VCHP at hot water temperature leaving the VCHP around 80 °C from the experimental results.

Table 4.2 Descriptions of each component of the two-stage VCHP.

Devices	Properties
Compressor R-134A (Reciprocating compressor, VCHP side)	Power input 3.70 A Displacement volume 20.30 m^3/h
Compressor R-123 (Scroll compressor, VCHP side)	Power input 1.50 A Displacement volume 14.92 m^3/h
Evaporator (Plate heat exchanger, VCHP side)	Capacity 6.00 kW Area 0.37 m^2
Condenser (Plate heat exchanger, VCHP side)	Capacity 10.00 kW Area 1.76 m^2
Economizer (Plate heat exchanger, VCHP side)	Capacity 8.00 kW Area 1.30 m^2
Expansion valve R-123 and R-134A (Thermo static orifice 02, VCHP side)	Capacity 10.00 kW Pressure ratio 3.00

Its EER_{VCHP} and power for compression work (W_{VCHP}) are found to be functions of the temperature difference between the water temperature entering the VCHP condenser ($T_{HW,i}$) and the water temperature entering the VCHP evaporator ($T_{CW,i}$) as shown in Figure 4.5, the empirical correlations could be found in the forms of

$$EER_{VCHP} = -0.037(T_{HW,i} - T_{CW,i}) + 4.4715, (kW_{th}/kW_e), \quad (4.3)$$

$$W_{VCHP} = 0.0129(T_{HW,i} - T_{CW,i}) + 2.3545, (kW_e). \quad (4.4)$$

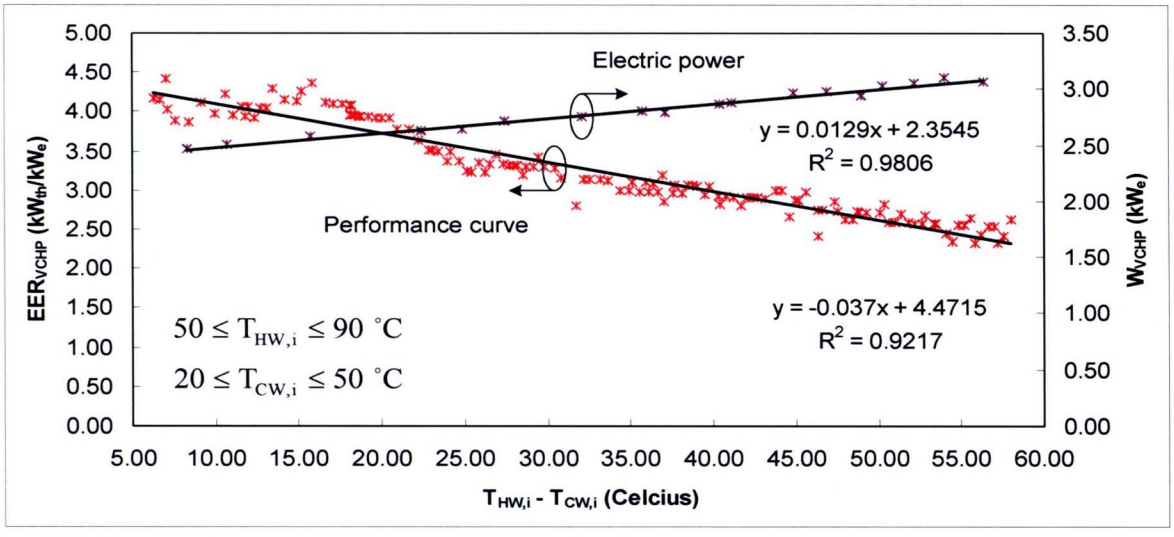

Figure 4.5 Performance curves of the R-134a/R-123 two-stage VCHP at hot water temperature leaving the VCHP around 80 °C from the experimental results.

Since the EER of the VCHP with the two-stage vapor compression heat pump is found to be higher than that with the single stage, therefore, the following section will consider only the performance of the AHT with the cascade vapor compression heat pump only.

Similarly, a simplified model of a constructed AHT used in the solar-CAHT as shown in Figure 4.6 is developed. The specifications of the AHT are given in Table 4.3 and the photographs of the constructed AHT components are shown in Figure 4.7.

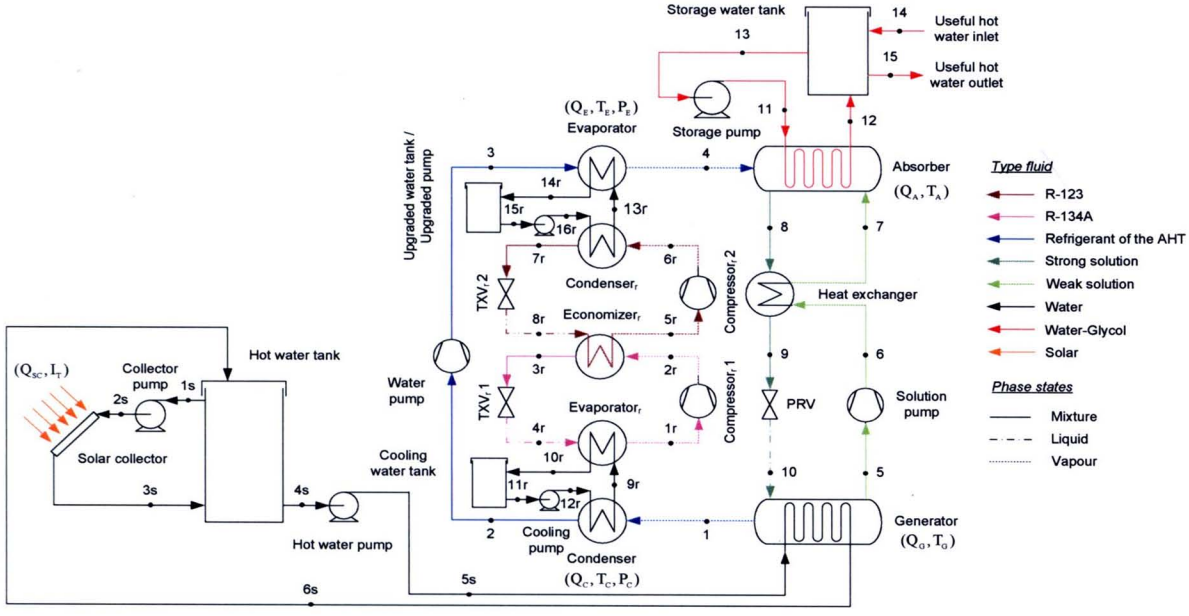

Figure 4.6 Schematic diagram of a solar absorption heat transformer coupling with a cascade VCHP.

Table 4.3 Descriptions of each component in the constructed solar-CAHT.

Devices	Properties
Flat-plate solar collector (Sanguantrakarnkul, 2006)	Area 2.3 m^2/unit $F_R(\tau\alpha) = 0.802$ $F_R U_L = 10.37\ W/m^2 \cdot K$
Generator (Flooded shell and tube heat exchanger, AHT side)	Capacity 10.3 kW Area 1.02 m^2
Condenser (Shell and tube heat exchanger, AHT side)	Capacity 10.6 kW Area 0.42 m^2
Absorber (Flooded shell and tube heat exchanger, AHT side)	Capacity 10 kW Area 1.44 m^2
Evaporator (Shell and tube heat exchanger, AHT side)	Capacity 10.8 kW Area 1.16 m^2
Hot water tank (Solar water heater)	Capacity 1,500 liter
Storage tank (AHT side)	Capacity 200 liter

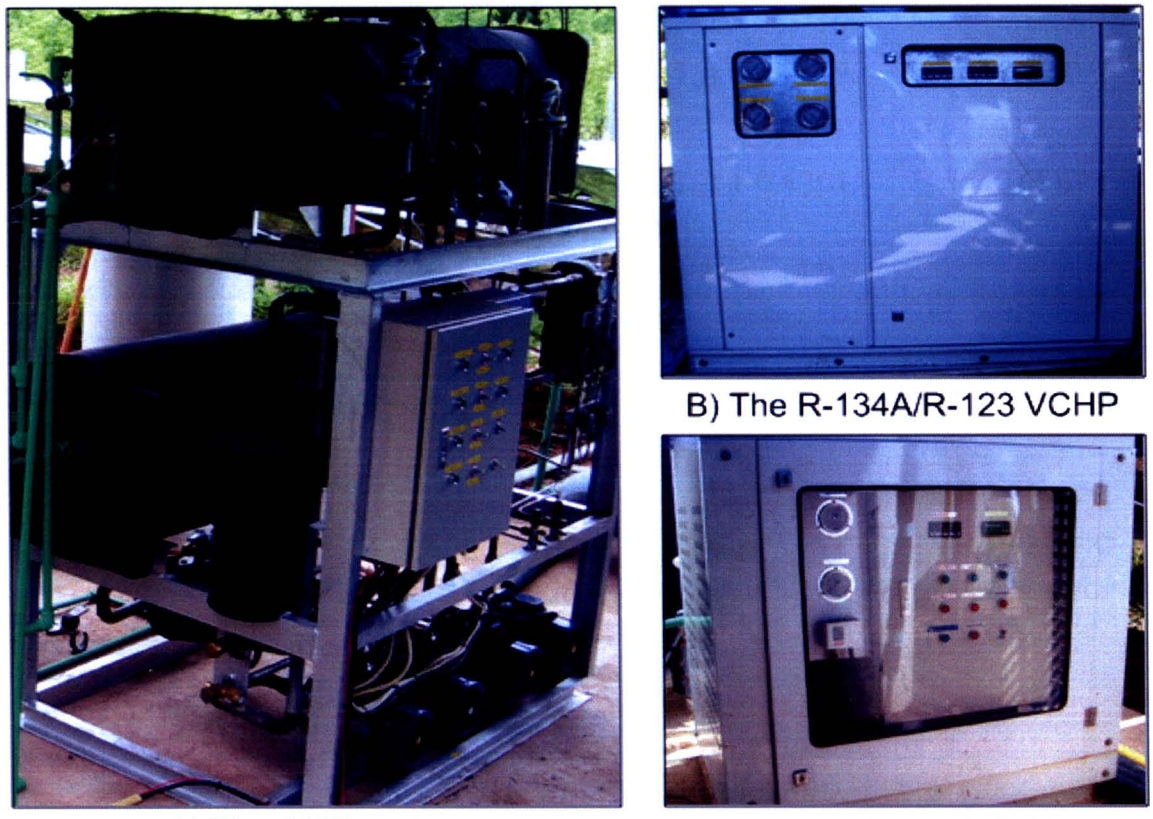

Figure 4.7 A Prototype of the AHT system, the R-134A/R-123 VCHP and the R-123 VCHP.

In the experiment, the water in a 200 liter is used to absorb heat at the AHT absorber. The investigation has been carried out when there is use and non-use of water in the tank. Since the temperature at the absorber is quite high then the water in the tank is mixed up with glycol with a composition of 40 % by volume.

Figure 4.8 shows COP_{AHT} and EER_{AHT} with $(T_{A,i} - T_E)/(T_{G,i} - T_C)$ when water in the storage tank (AHT side) was used and non-used.

In both cases, use and non-use of hot water, when the value of $(T_{A,i} - T_E)/(T_{G,i} - T_C)$ increased the COP_{AHT} and the EER_{AHT} decreased due to lower extracted heat at the absorber. When hot water was used, the COP_{AHT} and EER_{AHT} were higher than those of another case since the hot water temperature in the storage tank was lower thus the absorption could supply more heat. The empirical correlations of the COP_{AHT} with $(T_{A,i} - T_E)/(T_{G,i} - T_C)$ for both cases could be

For used hot water condition:

$$COP_{AHT} = -1.0444(T_{A,i}-T_E)/(T_{G,i}-T_C) + 0.7619. \quad (4.5)$$

For non-used hot water condition:

$$COP_{AHT} = -1.1434(T_{A,i}-T_E)/(T_{G,i}-T_C) + 0.6201. \quad (4.6)$$

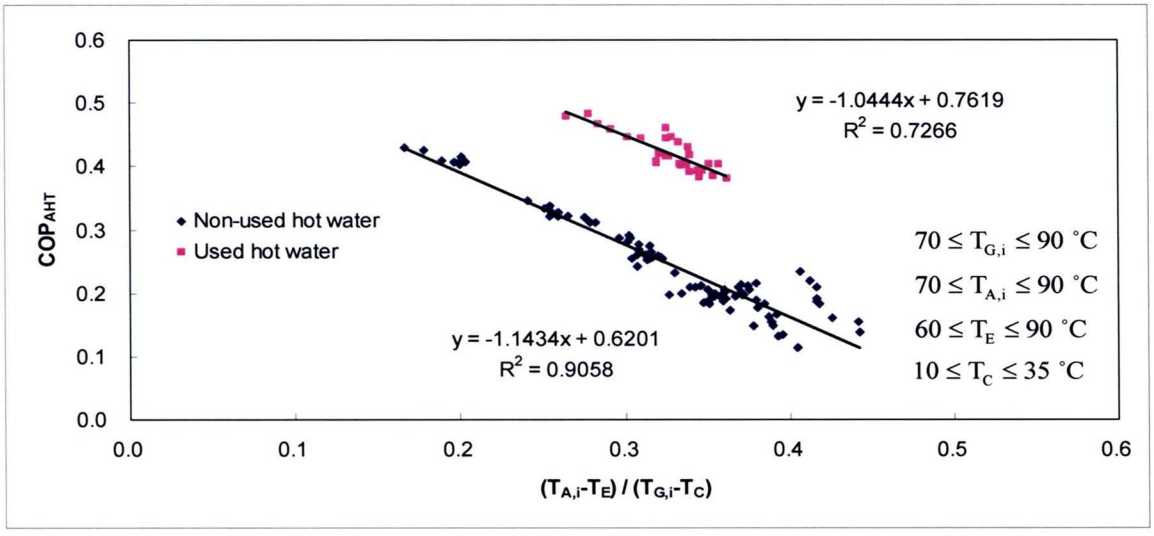

Figure 4.8 Effect of $(T_{A,i} - T_E)/(T_{G,i} - T_C)$ on COP_{AHT} of the AHT at hot water temperature leaving the AHT around 100 °C from the experimental results.

The empirical correlations of the EER_{AHT} ($\frac{\dot{Q}_A}{W_{elec}}$, kW_{th}/kw_{elec}) with $(T_{A,i} - T_E)/(T_{G,i} - T_C)$ for both cases could be

Similarly:

For used hot water condition:

$$EER_{AHT} = -10.463(T_{A,i}-T_E)/(T_{G,i}-T_C) + 7.5228. \quad (4.7)$$

For non-used hot water condition:

$$EER_{AHT} = -12.577(T_{A,i}-T_E)/(T_{G,i}-T_C) + 6.7079. \quad (4.8)$$

These equations are valid for the following criteria:

$$70 \le T_{G,i} \le 90\ ^\circ C,\ 70 \le T_{G,i} \le 90\ ^\circ C,$$

$$60 \le T_E \le 90\ ^\circ C,\ 10 \le T_C \le 35\ ^\circ C. \quad (4.9)$$

Figure 4.9 shows COP_{CAHT} with $(T_{A,i} - T_E)/(T_{G,i} - T_C)$ when water in the storage tank (AHT side) is used and non-used.

For used hot water condition:

$$COP_{CAHT} = -1.4741\ (T_{A,i}-T_E)/(T_{G,i}-T_C) + 1.0037. \quad (4.10)$$

For non-used hot water condition:

$$COP_{CAHT} = -1.6633\ (T_{A,i}-T_E)/(T_{G,i}-T_C) + 0.8476. \quad (4.11)$$

Similarly:

For used hot water condition:

$$EER_{CAHT} = -4.29\ (T_{A,i}-T_E)/(T_{G,i}-T_C) + 3.0883. \quad (4.12)$$

For non-used hot water condition:

$$EER_{CAHT} = -5.2404\ (T_{A,i}-T_E)/(T_{G,i}-T_C) + 2.784. \quad (4.13)$$

These equations are valid for the following criteria:

$$70 \le T_{G,i} \le 90\ ^\circ C,\ 70 \le T_{G,i} \le 90\ ^\circ C,$$

$$60 \le T_E \le 90\ ^\circ C,\ 10 \le T_C \le 35\ ^\circ C. \quad (4.14)$$

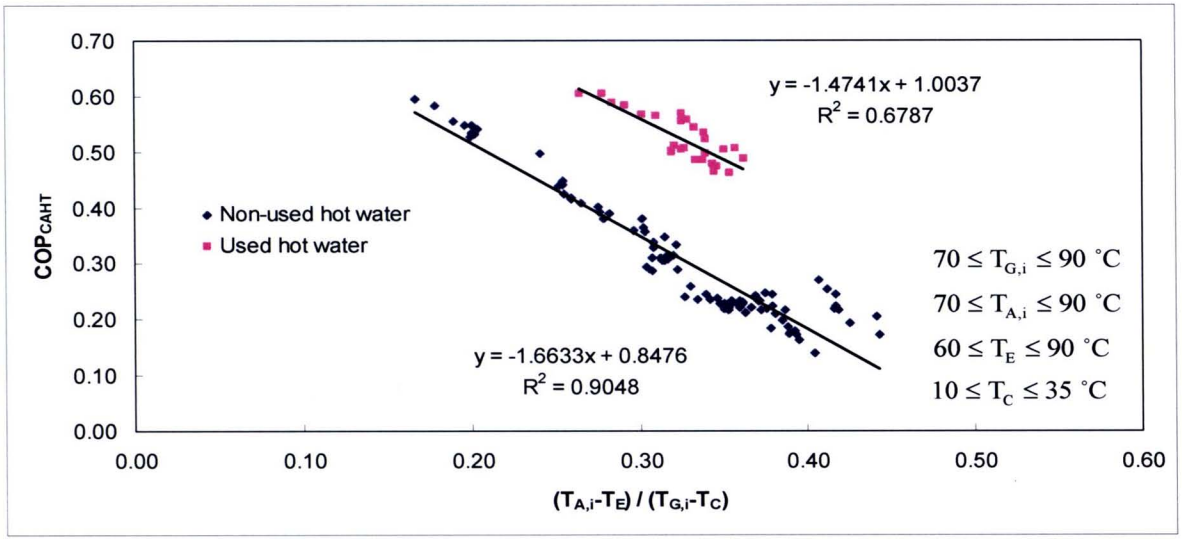

Figure 4.9 Effect of $(T_{A,i} - T_E)/(T_{G,i} - T_C)$ on COP_{CAHT} of the CAHT at hot water temperature leaving the AHT around 100 °C from the experimental results.

Figure 4.10 and Figure 4.11 show steps of calculation for the analyses of the VCHP and the AHT cycles with the simplified models. Performance correlations of the EER and the electrical power consumption with the operating temperatures are given. With the input data which are the operating conditions, the upgraded

temperature leaving the VCHP condenser and that leaving the AHT absorber are the outputs of the calculations, respectively.

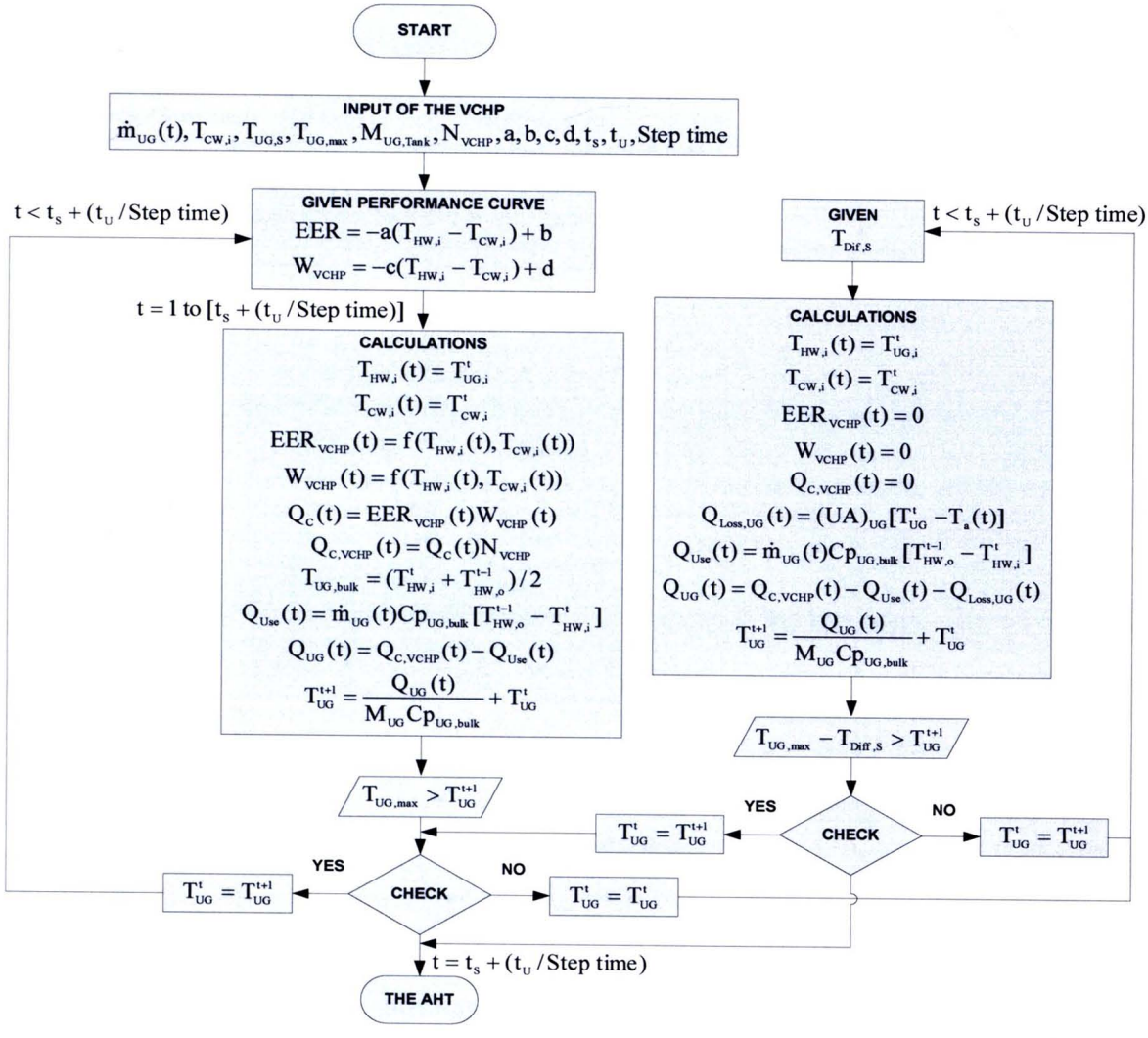

Figure 4.10 Flow chart for simulation of the vapor compression heat pump upgrading hot water temperature around 70-90 ˚C.

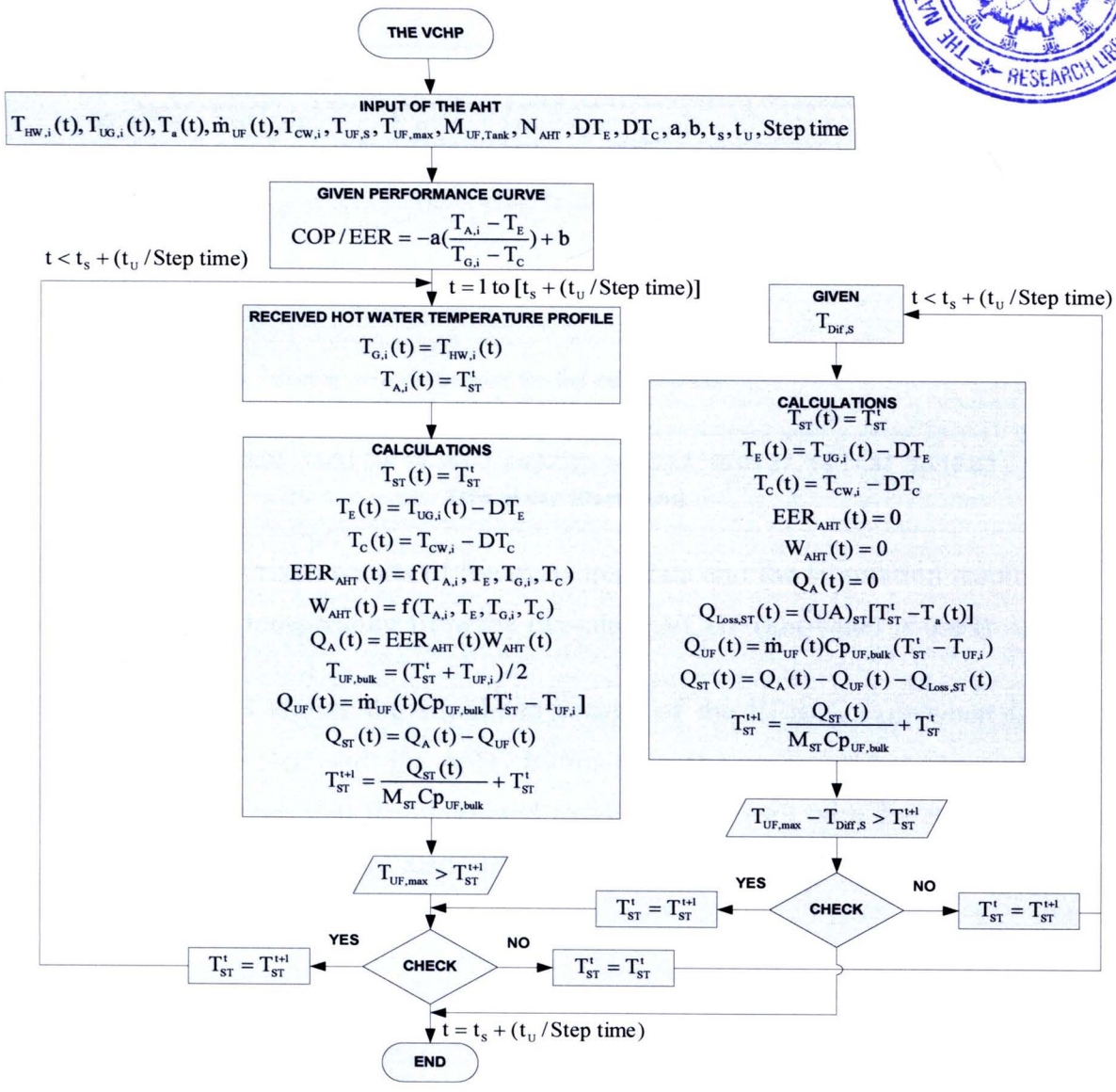

Figure 4.11 Flow chart for simulation of the absorption heat transformer upgrading hot water temperature around 90-110 °C.

4.5 Results and Discussion

The solar-CAHT as described above was tested. The EER of its VCHP was evaluated when the hot water of 200 liter at the AHT absorber was used at a heating capacity around 10 kW_{th}. The result was shown in Figure 4.12. It could be seen that the simulation results agreed well with those of the experimental data. Figure 4.12 also shows the water temperatures leaving the VCHP condenser and evaporator.

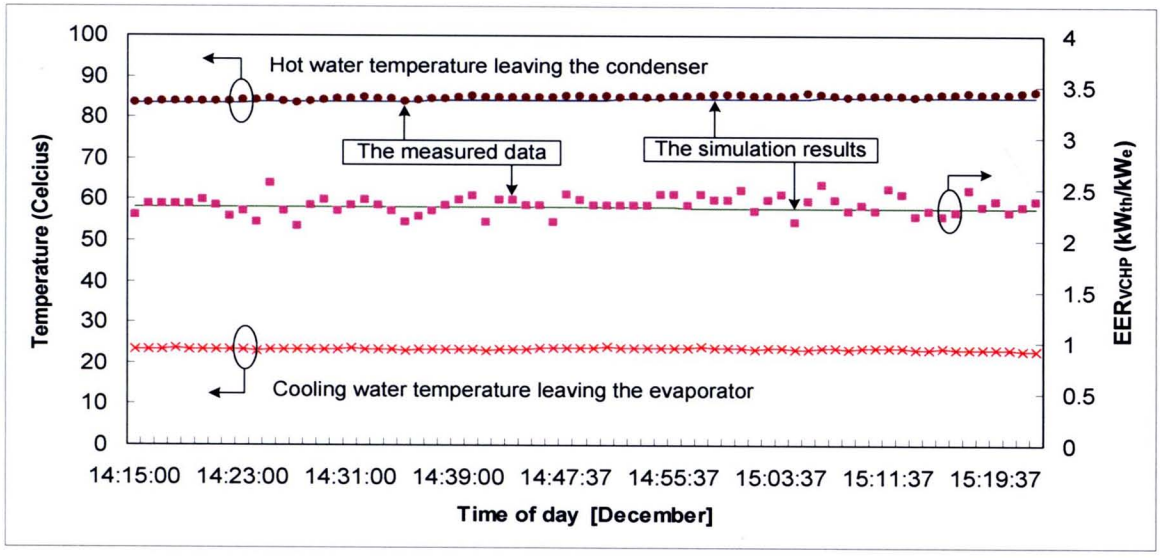

Figure 4.12 Comparison results of the measured data and the simulation results of hot water temperature from the two-stage VCHP (hot water is used).

Figure 4.13 shows the simulated results of the $EER_{solar\text{-}CAHT}$ when the two-stage VCHP is coupled with the AHT. In this case, the generated hot water was non-used. It could be seen that the simulated results agreed well with the measured data. The hot water temperature also affected the $EER_{solar\text{-}CAHT}$. As the temperature increased the EER decreased.

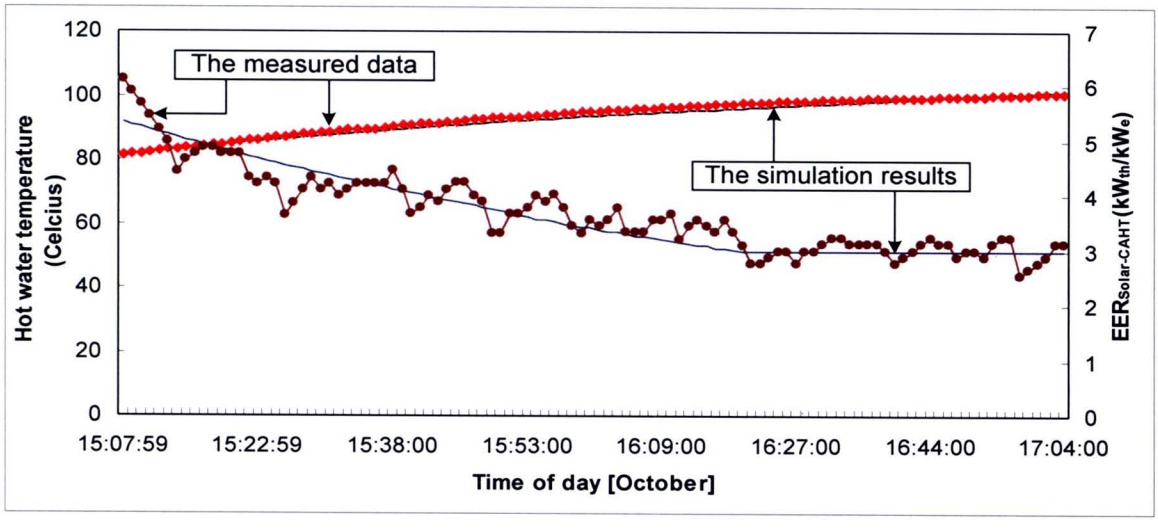

Figure 4.13 Comparison results of the measured data and the simulation results of hot water temperature from the solar-CAHT (hot water is not used of tank 200 liter).

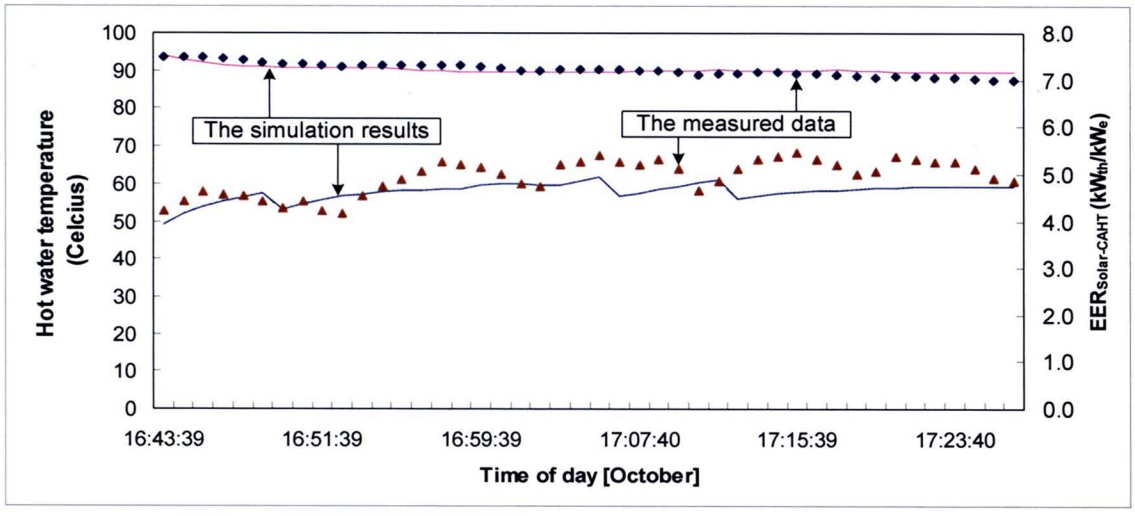

Figure 4.14 Comparison results of the measured data and the simulation results comparison of hot water temperature from the CAHT at flow rate 0.024 l/s (hot water is used at tank 200 liter).

Figure 4.14 also shows the $EER_{solar\text{-}CAHT}$ when the generated hot water is used at a flow rate of 0.024 l/s. It could be seen that when the hot water was used, the $EER_{solar\text{-}CAHT}$ was higher than that of the non-used hot water because the water temperature in the storage tank was lower then the system could supply more heat rate. In this Figure, the hot water temperature in the storage tank was nearly constant at 90 °C and the $EER_{solar\text{-}CAHT}$ was nearly constant at around 4.1. The simulated results agreed well with the measured data.

4.6 Conclusions

From this study, the conclusions are as follows:

1. From the simulation, the overall COPs of the solar-CAHT was around 0.71 compared with 0.49 of the normal solar-AHT. For the experimental results, the overall COPs of solar-CAHT and the solar-AHT were around 0.62 and 0.39, respectively.
2. The simplified models of the two-stage VCHP and the AHT could be used to predict the thermal performances of the solar-CAHT. The simulated results agreed well with experimental data.